Hladuvka2024a

Fitting Egg-Shapes to Discretized Object Boundaries

Jiří Hladůvka(✉) and Walter G. Kropatsch

Institute of Visual Computing and Human-Centered Technology, TU Wien, Vienna, Austria

jiri@prip.tuwien.ac.at

Abstract. This paper presents a novel method for fitting egg-shapes to discrete sets of boundary points. Egg-shapes extend ellipses by assigning a positive weight to one of the two focal points. Fitting of egg-shapes thus requires optimization of 6 parameters. Our approach simplifies this to a 1D parameter space exploration. First, we utilize a least square algorithm to fit an ellipse to the boundary. While the desired egg-shape shares the orientation of the major axis and to a certain extent also the size of the ellipse, its fine-tuning to the boundary is more involved than merely adjusting the focal weight. To this end, we establish a relation between the eccentricity of the ellipse and the two shape-defining parameters of the closest egg-shapes. Subsequently, we utilize this relationship to iterate over a 1D space of closest egg-shape candidates while assessing their fitness to the boundary. Our results underscore the benefits of using egg-shapes over ellipses for representing a spectrum of real-world objects.

Keywords: egg-shape · fitting · discrete shape · eccentricity · ellipse · generalized conics

1 Introduction

The core task in any computer vision problem is to define and efficiently express the essential object characteristics [11]. In order to represent a shape, one strategy is to approximate it by fitting a geometric primitive to the set of its boundary points. For example, an ellipse enables describing the 2D shape by elongation and orientation and requires 5 parameters. This significantly simplifies the processing and memory costs compared to the entire collection of pixels [1]. As a result, ellipse fitting is an area of extensive research [2,5,12,17] and finds its use in a multitude of applications [7,9,10,14].

This paper presents an advancement in the field of shape representation by exploring the potential of an egg-shape [3]. This generalization of the ellipse introduces a positive weight to one of the focal points. Despite the broadened scope of objects that might be described by egg-shapes, there are two key areas that have not been addressed to the best of our knowledge. Firstly, there is a lack of real-world examples demonstrating the benefits of egg-shapes. Secondly, it is

S. Brunetti et al. (Eds.): DGMM 2024, LNCS 14605, pp. 107–119, 2024.
https://doi.org/10.1007/978-3-031-57793-2_9

the absence of a method for fitting egg-shapes to object boundaries. To this end, existing literature provides fitting methods for a different generalization, i.e., the super-ellipse [8,18], that yields shapes from four-armed stars with concave sides to rectangles thru an additional parameter.

Addressing these gaps, we have identified various classes of real-world objects, such as chicken eggs, avocados, leaves, spoons, and rackets, that demonstrably benefit from egg-shape representation. We have assembled a collection of 1337 such objects, complete with photographs and boundaries, and have made this collection publicly accessible [15] in conjunction with the publication of this paper. A selection of four boundaries from this collection is presented in the results Sect. 6.

Crucially, we have developed an algorithm, detailed in Sect. 4, that is capable of fitting egg-shapes to the discretized boundaries of these objects. The research code for this algorithm has also been made publicly available [6].

The primary contribution of our work, detailed in Sect. 3, is the reduction of the search space from six parameters to a single one. This was enabled by our key discovery, i.e., the relationship between egg-shape parameters and the eccentricity of its best-fitting ellipse. This contribution was facilitated by addressing two crucial aspects of the egg-shape: its *explicit*, polar-form representation (sec. 2.1) and the derivation of its arc-length sampling (sec. 2.2).

2 Egg-Shapes

Conics have been generalized by assigning real-valued weights w_i to multiple focal points F_i in higher-dimensional metric spaces [4]. These generalizations are elegantly encompassed by $\Sigma_i w_i \|P - F_i\| = c \in \mathbb{R}$, which implicitly defines the conic by its points P.

In this work, we focus on shapes in the Euclidean plane induced by two foci and two positive weights. After a weight normalization [3], we are left with a single weight μ from the unit interval.

Definition 1 (Egg-shape). *Given two distinct foci $F_0 \neq F_1$ in the Euclidean plane, weight $0 \leq \mu \leq 1$, and scaling factor $c \geq 1$.* Egg-shape *is a set of points P in the Euclidean plane fulfilling*

$$d_0 + \mu d_1 = c \cdot f \tag{1}$$

where $d_i = \|P - F_i\|$ are the distances of P from foci F_i and $f = \|F_1 - F_0\|$ is the focal distance.

Wherever context permits, we may use the term *egg* as a shorthand for egg-shape. Definition 1 encompasses circles ($\mu = 0$), ellipses ($\mu = 1$), as well as a spectrum of egg-like shapes with various sharpness (Fig. 5), including those with sharp corner [3] at $c = 1$ (Fig. 3).

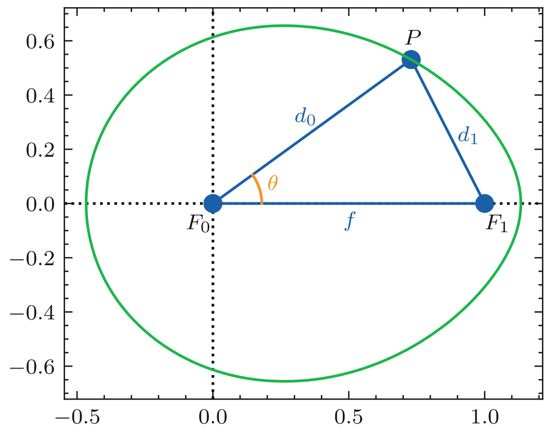

Fig. 1. Deriving polar coordinates. Unit egg U_{01} parametrized by $c = 1.2$, $\mu = 0.5$.

2.1 Polar Coordinates

To explicitly express the egg in polar coordinates, we consider the two foci at the origin $F_0 = [0, 0]^\top$ and on the positive horizontal axis, $F_1 = [f, 0]^\top$. Setting the focal distance $f = 1$ yields what we refer to as the unit egg U_{01} (Fig. 1). Later, we will also refer to its left-oriented counterpart U_{10} flipped about $x = 1/2$.

For any point P at angle θ on the egg (1) holds. Taking the square results in:

$$d_1^2 = \left(\frac{cf - d_0}{\mu}\right)^2 \tag{2}$$

Furthermore, the law of cosines yields:

$$d_1^2 = d_0^2 + f^2 - 2d_0 f \cos(\theta) \tag{3}$$

Subtracting (3) from (2) results in quadratic equation in d_0:

$$d_0^2\left(\mu^2 - 1\right) + d_0\left(2f(c - \mu^2\cos(\theta))\right) + f^2\left(\mu^2 - c^2\right) = 0. \tag{4}$$

For $\mu = 1$ the quadratic term vanishes yielding the polar equation of an ellipse. For $\mu = 0$, $d_0 = cf$ implicitly defines points P on a circle centered at F_0. For $0 < \mu < 1$ and fixed θ, the two solutions of (4), i.e.,

$$d_0^+, d_0^- = f \cdot \frac{\mu^2\cos(\theta) - c \pm \mu\sqrt{c^2 - 2c\cos(\theta) - \mu^2\sin^2(\theta) + 1}}{\mu^2 - 1} \tag{5}$$

correspond to distances (from F_0) of two points: P on the egg ($\mu > 0 \Rightarrow d_0^+$), and P^- on a generalized hyperbola ($\mu < 0 \Rightarrow d_0^-$) [3], which is further not discussed. Putting $r(\theta) = d_0^+$ yields the polar coordinates $(r(\theta), \theta)$ of the egg-shape.

2.2 Arc Length

Similar to ellipses, uniform sampling of the polar angle θ will generally lead to uneven distribution of points on the boundary (Fig. 3, left). Such sampling would likely introduce bias when fitting to the discretized boundary of an object.

To address undersampled segments, we aim at the arc-length parameterization (Fig. 3, right). Computing the arc-length L between two angles $\theta_0 < \theta_1$ in the polar parametrization (r, θ) involves numerical integration of:

$$L(\theta_0, \theta_1) = \int_{\theta_0}^{\theta_1} \sqrt{r^2 + \left(\frac{dr}{d\theta}\right)^2} d\theta \tag{6}$$

Putting

$$R = R(\theta) = \sqrt{c^2 - 2c\cos(\theta) - \mu^2 \sin^2(\theta) + 1} \tag{7}$$

$$M = M(\theta) = \mu^2 \cos(\theta) - c \tag{8}$$

$$A = \mu^2 - 1 \tag{9}$$

simplifies the terms for r and its derivative w.r.t θ to:

$$r = f \cdot \frac{M + \mu R}{A} \tag{10}$$

$$\frac{dr}{d\theta} = -f \cdot \frac{M + \mu R}{A} \cdot \mu \cdot \frac{\sin(\theta)}{R} = -r \cdot \mu \cdot \frac{\sin(\theta)}{R} \tag{11}$$

Equation (11) confirms the discovery regarding the sharp corners [3] in eggs with $c = 1$ (Fig. 3). Specifically, when $c = 1$, $R(\theta)$ vanishes at $\theta = 2k\pi \ \forall k \in \mathbb{Z}$, which results in discontinuities in $dr/d\theta$ and leaves the derivatives undefined. However, $dr/d\theta$ is an odd function with finite and opposing left/right limits in $2k\pi$:

$$\lim_{\substack{c=1 \\ \theta \to 2k\pi^-}} -r\mu \frac{\sin(\theta)}{R} = \frac{r\mu}{\sqrt{1-\mu^2}} = - \lim_{\substack{c=1 \\ \theta \to 2k\pi^+}} -r\mu \frac{\sin(\theta)}{R} \tag{12}$$

Therefore, the square $(dr/d\theta)^2$ in (6) exists in the limit (from either side):

$$\lim_{\substack{c=1 \\ \theta \to 2k\pi}} \left(\frac{dr}{d\theta}\right)^2 = \frac{r^2\mu^2}{1-\mu^2} \tag{13}$$

Equations (10)–(13) result, for given θ, in a recipe to reuse the radius r to compute the square of the derivative. Having the ingredients, the values of arc-length $L(0, \theta)$ can be utilized to sample the egg points at regular distances as exemplified in Figs. 2 and 3.

3 Egg-Shapes and Best-Fitting Ellipses

We aim to establish the correspondence between egg parameters and the eccentricity $\varepsilon = \varepsilon(c, \mu)$ of the best-fitting ellipse [5]. Two bounding cases are apparent from the equation for egg-shape (cf. Fig. 4):

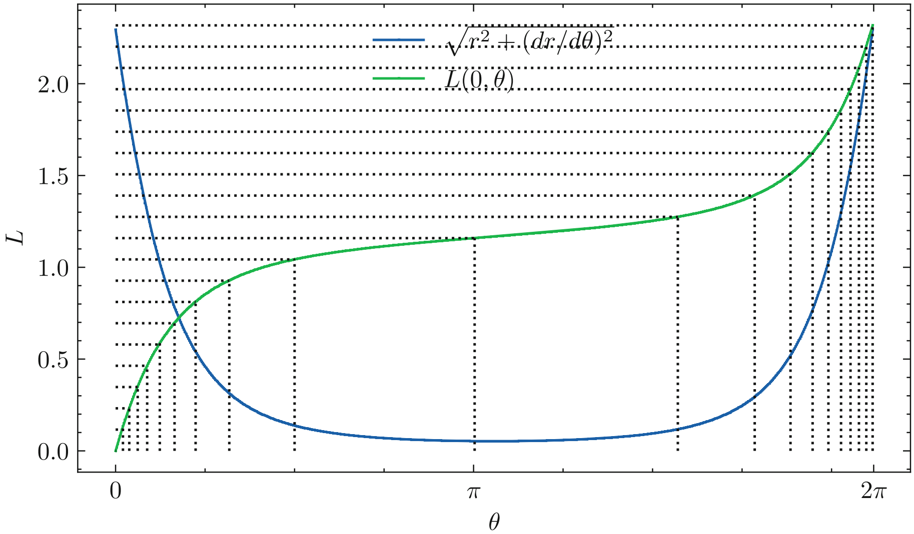

Fig. 2. Uniform sampling along the arc length L (horizontal lines) leads to samples of θ (vertical lines), which correspond to the equidistant sampling of the egg-shape.

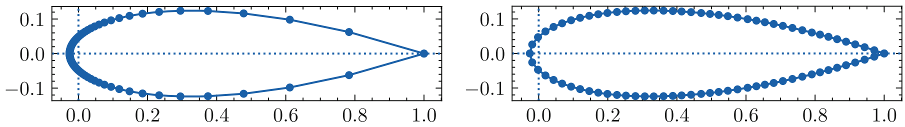

Fig. 3. A corner-egg ($c = 1$) with θ sampled linearly (left) and by arc length (right).

$\varepsilon(c, 0) = 0/c$: egg-shape, and thus also its best-fitting ellipse, is a circle implicitly given by $d_0 = cf$.

$\varepsilon(c, 1) = 1/c$: egg-shape, and thus also its best-fitting ellipse, is an ellipse implicitly given by $d_0 + d_1 = cf$, i.e., one with focal distance f, the length of its main axis cf, and eccentricity $\varepsilon = f/(cf) = 1/c$.

To model $\varepsilon(c, \mu)$ between, we fitted ellipses by the robust algorithm [5] to the sampled boundaries of unit eggs parametrized by $\mu \in (0, 1)$ and $c \in \langle 1, 5 \rangle$.[1] This way we densely sampled the parameter space of egg-shapes and tracked the fitting-ellipse eccentricities.

Interestingly, this process reveals a power-rule increase of ε w.r.t. μ. This is illustrated in Fig. 4 by the two dotted lines at $c = 1$ and $c = 5$. The power-rule behavior becomes apparent after the scaled $\varepsilon \cdot c$ curves map to lines through the origin in a log-log plot. Moreover, it can be observed that the slopes S of the log-log lines are inversely proportional to c, $S \propto 1/c$.

[1] The upper bound for c was determined by the expected lowest eccentricity of ellipses fitted to modeled objects. For our collection [15]: $c_{\max} = 1/\varepsilon_{\min} \leq 1/0.2 = 5$.

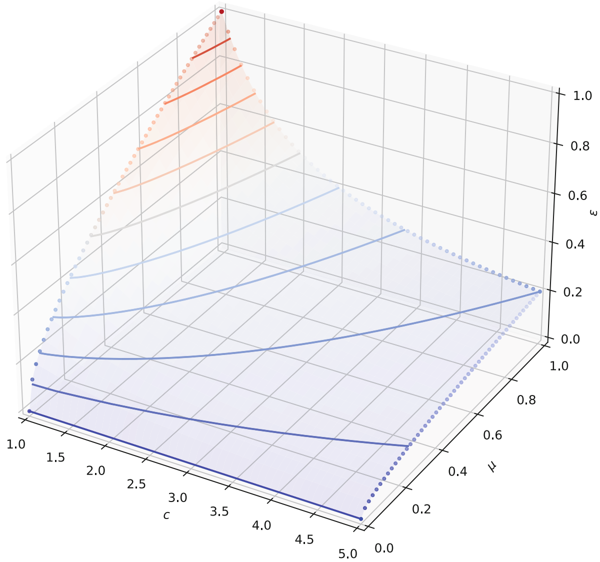

Fig. 4. Relationship between egg-shape parameters c, μ, and the eccentricity of the best-fitting ellipse. The ten solid curves correspond to iso-eccentricity lines (blue at 0, red at 0.9). The red dot at $(c,\mu) = (1,1)$ corresponds to the unit eccentricity of the degenerated case, i.e., the line connecting the two foci. (Color figure online)

This encourages to model the eccentricity by

$$\varepsilon(c,\mu) \approx \frac{1}{c} \cdot \mu^{S(c)} \tag{14}$$

where

$$S(c) \approx S(c;\alpha,\beta,\gamma) = \beta + \frac{\alpha}{c+\gamma} \tag{15}$$

Fitting the three parameters results in $\alpha = 0.01994611$, $\beta = 0.49646579$, $\gamma = -0.7994735$ and yields an error in eccentricity of 0.0000 ± 0.0013.

It is worth mentioning that this modeling is performed only once, before fitting egg-shapes to object boundaries.

4 Fitting Egg-Shapes via an Ellipse Proxy

Equation (14) relates the eccentricity of best-fitting ellipse given egg-shape parameters. More importantly, we can constrain the inverse, egg-to-ellipse fitting problem to the iso-eccentricity line in the (c,μ) space (Fig. 5).

Given an ellipse of eccentricity ε, the parameter c is restricted to the interval $\langle 1, 1/\varepsilon)$. Rewriting (14) allows, for a fixed c, computation of the corresponding μ:

$$\mu = \mu(c;\varepsilon) = (c \cdot \varepsilon)^{1/S(c)} \approx (c \cdot \varepsilon)^{\frac{(c+\gamma)}{\beta(c+\gamma)+\alpha}} \tag{16}$$

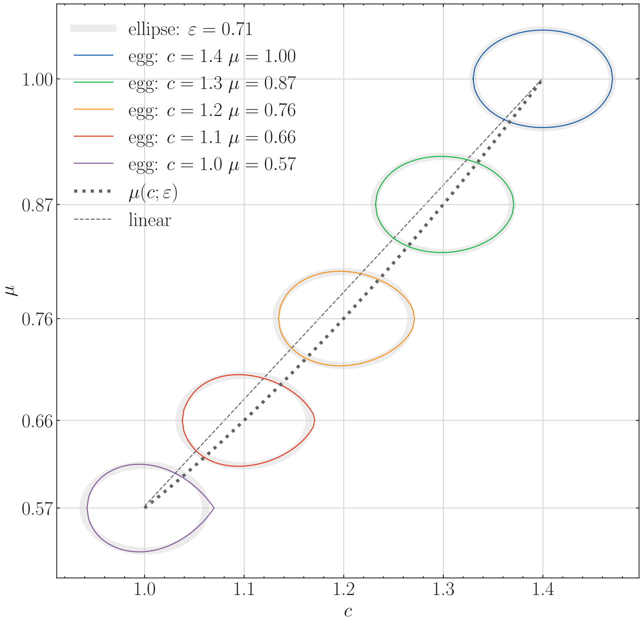

Fig. 5. Sampled best-fitting eggs to an ellipse of fixed eccentricity on the curve given by Eq. (16) in the (c, μ) parameter space. For clarity, the unit eggs are scaled down.

Our objective is to fit an egg-shape to a segmented object represented by boundary points B. It is important to note that, unlike the unit egg, boundaries B can be arbitrarily placed and oriented within the Euclidean plane.

The steps of Algorithm 1 proceed as follows: We begin by fitting a *proxy* ellipse to the boundary points B and recording its eccentricity. It is worth noting that while the proxy provides the angle of the object's main axis, it does not disambiguate between the two possible orientations of the object's tip. Next, we perform an iterative search along the iso-eccentricity curve. During each iteration, we fit ellipses to both the arc-sampled unit egg U_{01} and its horizontally flipped counterpart U_{10}. Since both ellipses share the same eccentricity as the proxy, they naturally determine transformations that align U_{01} and U_{10} with the boundary B. Finally, we resolve the object's tip orientation by assessing both transformed eggs by fitness to the boundary B using a metric Δ. In the context of this paper, Δ represents the average Hausdorff distance defined later in Sect. 5.

Algorithm 1. Fitting egg to boundary along 1D iso-eccentricity curve

Require: B ▷ boundary coordinates of egg-like object

$E_B \leftarrow$ fit_ellipse (B) ▷ fit a proxy ellipse to the boundary

$\varepsilon_B \leftarrow$ eccentricity (E_B) ▷ eccentricity to restrict the search

$(\Delta^*, F_0^*, F_1^*, c^*, \mu^*) \leftarrow (\infty, [0,0]^\top, [1,0]^\top, 1, 0)$ ▷ loss, foci, and params to optimize

for $c \in \langle 1, 1/c)$ **do** ▷ sample the iso-eccentricity curve

  $\mu \leftarrow \mu(c; \varepsilon_B)$ ▷ equation (16)

  $U_{01} \leftarrow$ unit_egg (c, μ) ▷ unit egg given by c, μ

  $U_{10} \leftarrow$ flip (U_{01}) ▷ unit egg flipped about $x = 1/2$

  for $o \in \{0, 1\}$ **do** ▷ for both orientations of the unit egg

    $E_U \leftarrow$ fit_ellipse $(U_{o,1-o})$ ▷ ellipse fitting the unit egg, $ecc(E_U) \approxeq ecc(E_B)$

    $T_{UB} \leftarrow \text{argmin}_T |T(E_U), E_B|$ ▷ E_U to proxy alignment transform

    $G \leftarrow T_{UB}(U_{o,1-o})$ ▷ bring the egg to the object boundary

    $\Delta \leftarrow |G, B|$ ▷ distance of the transformed egg to the boundary

    if $\Delta < \Delta^*$ **then** ▷ if loss decreased

      $(\Delta^*, F_0^*, F_1^*, c^*, \mu^*) \leftarrow \left(\Delta, T_{UB}([o,0]^\top), T_{UB}([1-o,0]^\top), c, \mu\right)$ ▷ update

    end if

  end for

end for

return $(F_0^*, F_1^*, c^*, \mu^*)$ ▷ foci and parameters of the best-fitting egg

5 Validation

Our methodology is verified using both overlap-centric and distance-centric metrics [16] on a purposely created collection of boundaries [15] segmented from images of both biological and common objects. These include both deformable and rigid items captured in arbitrary orientations and scales. Each segmentation is represented by a binary mask and its boundary thus as a set of integer coordinates.

5.1 Datasets

Whole eggs: Boundaries of 1,100 photographed eggs [13].

Boiled eggs: Images of longitudinally halved, hard-boiled eggs found on the internet were manually segmented, yielding 12 boundaries each for the egg whites and yolks.

Avocados: Images of longitudinally halved avocados were found on the internet. The shells of these avocados were manually segmented, resulting in 6 boundaries. Some of them are slightly deformed.

Leaves: Tree and plant leaves were deliberately selected and photographed in line with this study. The criteria included being longitudinally symmetrical, egg-shaped, elongated, and possibly pointed. Manual segmentation excluded the stems and produced 23 boundaries.

Cells: Palisade cells of Arabidopsis thaliana in a micro-CT cross-section slice were manually segmented, resulting in 159, mostly elliptic boundaries.

Household items: 11 spoon heads and 2 toilet seats segmented from photos.

Rackets: Images of tennis, badminton, and squash racket heads sourced from the internet were segmented, resulting in 12 boundaries. The outer shell of the squash head is noted to be pointed. One of the tennis heads is elliptic.

5.2 Validation Metrics

The geometric alignment of a model with the object boundary is evaluated using metrics that take into account either the boundary point sets M and B, or the corresponding polygons $\mathbf{M}$ and $\mathbf{B}$.

IoU (also referred to as the Jaccard index) [16], defined as the area of the intersection divided by the area of the union of polygons $\mathbf{M}$ and $\mathbf{B}$:

$$IoU(M, B) = \frac{|\mathbf{M} \cap \mathbf{B}|}{|\mathbf{M} \cup \mathbf{B}|} \tag{17}$$

ranges from 0 to 1, with 1 indicating perfect alignment.

The Average Hausdorff Distance ($\overline{HD}$) is used to assess the fitness for its decreased sensitivity to outliers [16] when compared to the usual Hausdorff distance. $\overline{HD}$ is defined by:

$$\overline{HD}(M, B) = \max\left(d(M, B), d(B, M)\right) \tag{18}$$

where d(X, Y) is the *directed* Average Hausdorff distance [16] given by:

$$d(X, Y) = \frac{1}{|X|} \sum_{x \in X} \min_{y \in Y} ||x - y||. \tag{19}$$

To assess improvements of egg models M_G over elliptic models E_L across contours of different lengths we further introduce the following normalization:

Normalized Improvement (NI) in average Hausdorff distance $\overline{HD}$ of egg model M_G over elliptical model M_L when fitted to boundary B. We define $NI = 0$ if models align. Otherwise:

$$NI(M_G, M_L|B) = \frac{\overline{HD}(M_L, B) - \overline{HD}(M_G, B)}{\max\left(\overline{HD}(M_L, B)\ ,\ \overline{HD}(M_G, B)\right)}. \tag{20}$$

Being already normalized, IoU is naturally suited to assess improvements by:

$$\Delta IoU(M_G, M_L|B) = IoU(M_G, B) - IoU(M_L, B). \tag{21}$$

Both improvement metrics fall in the closed interval $\langle -1, 1\rangle$. Positive values indicate an improvement due M_G, while negative values signify a decline.

6 Results

Figure 7 showcases a selection of top-improvement examples. To avoid clutter, Fig. 6 summarizes both improvement metrics (20), (21) in two separate scatter plots. 94.68% of data points indicating improvements in both metrics are located in the 1^{st} quadrants. The ties in the 2^{nd} and 4^{th} quadrants correspond to cases improved in only one of the metrics. They account for $10+11$ out of 159 cells and $9+12$ out of 1100 whole eggs. Finally, the 3^{rd} quadrant shows minimal declines in both metrics: less than 4% of cells (6 out of 159) and less than 2% of whole eggs (20 out of 1100). The leftmost point of the upper part is the elliptic tennis racket that can not be improved by the egg-shape.

In the marginal-improvement rectangle $(0, 0.1) \times (0, 0.02)$ in the upper part, a cluster of 9 boiled-egg yolks can be found. They are almost elliptical making it difficult for the egg-shapes to improve them. This explains the almost identical *IoU* and only marginally improved *NI* values. The enclosed badminton racket already deviates from an ellipse and was slightly improved by an egg-shape.

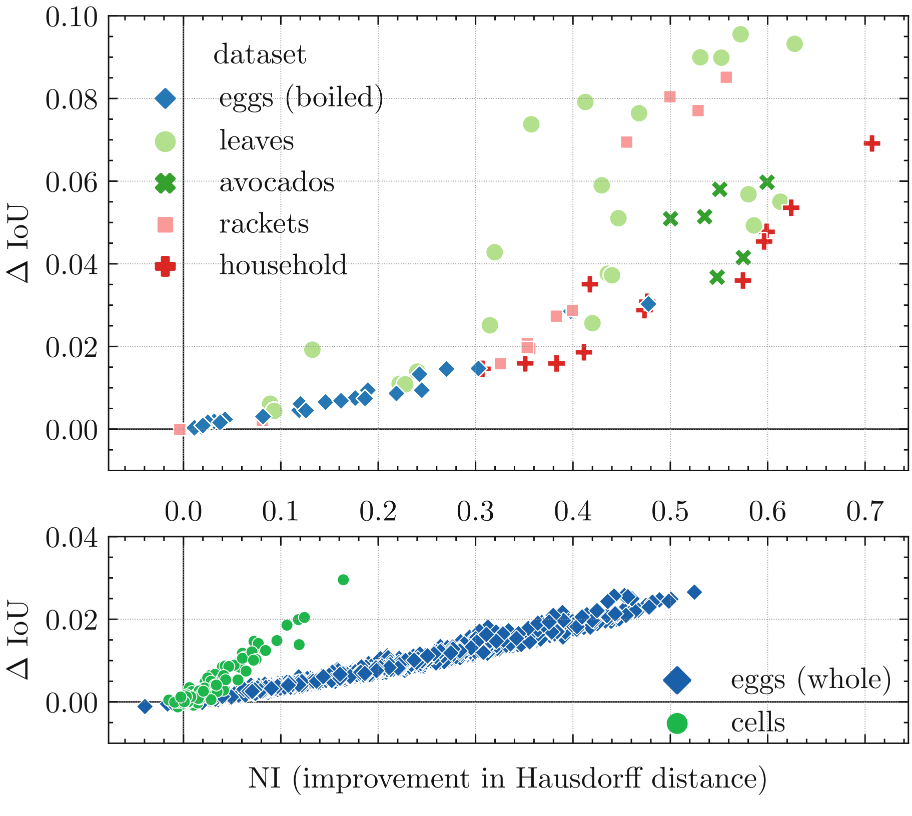

Fig. 6. Normalized improvements in average Hausdorff distance (*NI*) and in *IoU*.

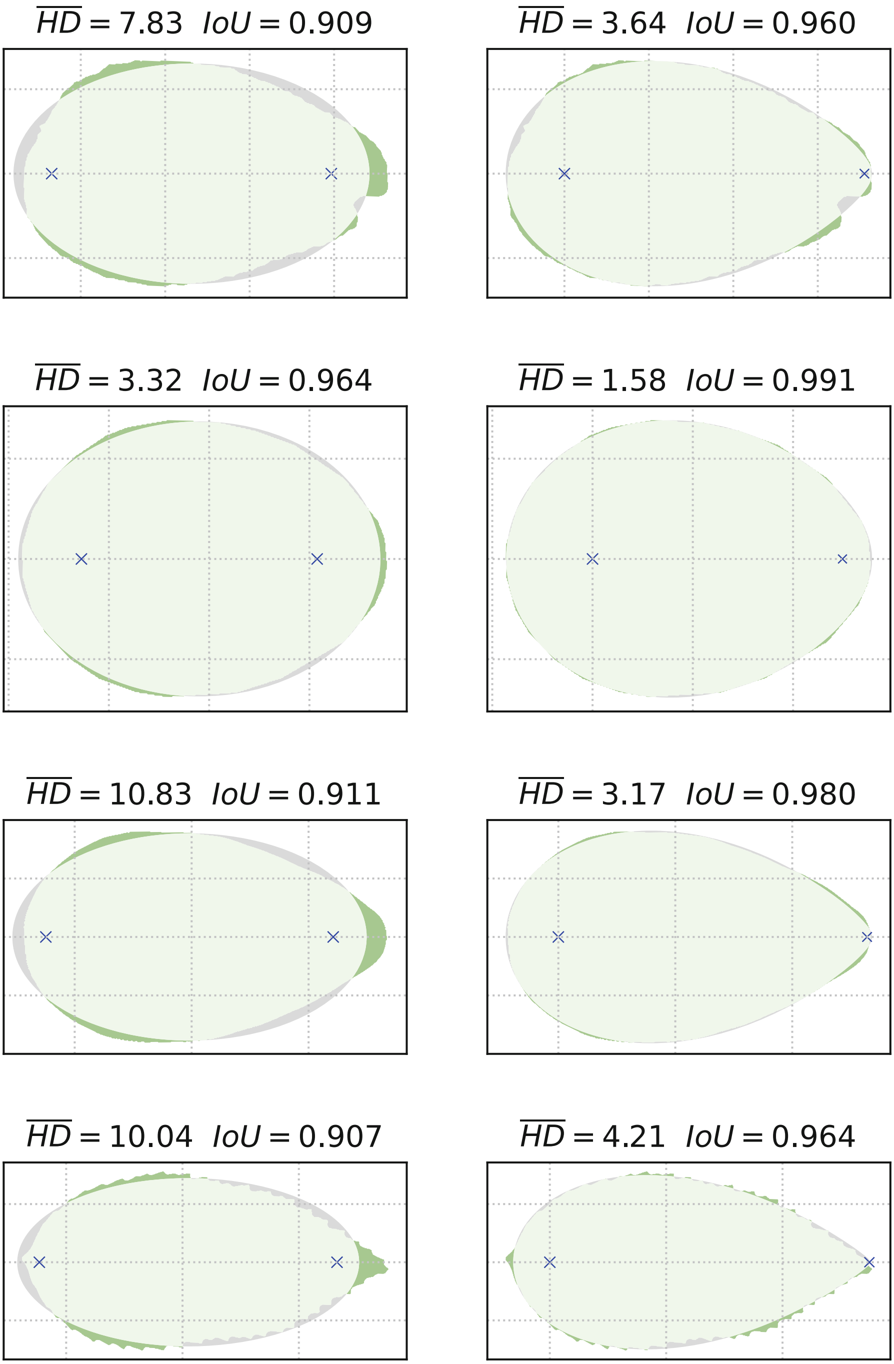

Fig. 7. Improvements by egg-shape fit (right column) over elliptic fit (left column) for selected contours. Top to bottom: avocado ($NI = 0.54$), whole egg ($NI = 0.52$), spoon head ($NI = 0.71$), and leaf ($NI = 0.58$). Gray and dark green areas are not explained well by the respective model. The blue crosses show the foci. (Color figure online)

Upon examining areas with higher improvements, it becomes apparent that the term *egg*-shapes may warrant reconsideration. In our selection, avocados outperformed eggs (both boiled and whole) in both metrics. This can be attributed to their more tapered shape, which is better modeled by egg-shapes.

A similar observation can be made about the top-scoring leaves (e.g., those with $\Delta IoU \gtrsim 0.06$) and spoons ($NI \gtrsim 0.6$), which are difficult to model using ellipses. However, egg-shapes have proven effective in modeling the spikes or even sharp corners by reducing c towards 1 (refer to Fig. 7).

In the bottom part of Fig. 6, most of the plant cells cluster in the marginal improvement rectangle. This is because most of the cells are elliptical or even circular in shape, and an ellipse already provides a good model. A strong correlation between the metrics is evident for both datasets. Unlike eggs, the cells have been segmented from a single image, which results in more jagged boundaries. For such boundaries, improvements in IoU could potentially be more pronounced than those in NI, explaining the steeper trend.

7 Conclusions and Future Work

In this paper, we introduced a novel method for fitting discrete boundaries using egg-shapes. We ventured beyond the confines of implicit equations and harnessed the power of explicit representation in conjunction with arc-length parametrization. This approach led to our key finding: a relationship between egg-shape parameters and the eccentricity of the best-fitting ellipse, which subsequently informed the design of our fitting algorithm.

Our algorithm was rigorously tested on over 1,000 boundaries. The results have demonstrated the potential of egg-shapes for representing real-world objects. Unexpectedly, we have discovered that there are objects other than *eggs*, which when fitted with an *egg*-shape, show even better improvements over elliptic fits. This intriguing finding expands the potential applications of egg-shape fitting beyond what was initially anticipated.

The results of our research pave the way for future development, which can be pursued along several avenues: 1. The choice of arc-length parametrization was largely based on intuition. A comparison with its linear counterpart is necessary to validate our approach. 2. Our algorithm currently performs an exhaustive search along the iso-eccentricity curve. However, the existence of a global minimum along this curve, which could potentially speed up the fitting process, remains unexplored. 3. Similar to egg-shape parameters, we observed a promising pattern between eccentricity and the offsets of the focal points. However, modeling this seems to be a more complex task. 4. We have yet to address the robustness of our method in dealing with noise, overlaps, or partial occlusions.

Acknowledgements. We would like to express our sincere gratitude to Aysylu Gabdulkhakova for sharing her invaluable insights and knowledge on egg-shapes.

This project was supported by the Vienna Science and Technology Fund (WWTF) project LS19-013 and the Vienna Scientific Cluster (VSC).

References

1. Costa, L.D.F., Cesar, R.M., Jr.: Shape Analysis and Classification: Theory and Practice. CRC Press, Boca Raton (2000)
2. Fitzgibbon, A., Pilu, M., Fisher, R.: Direct least square fitting of ellipses. IEEE Trans. Pattern Anal. Mach. Intell. **21**(5), 476–480 (1999)
3. Gabdulkhakova, A., Kropatsch, W.G.: Generalized conics with the sharp corners. In: Progress in Pattern Recognition, Image Analysis, Computer Vision, and Applications, pp. 419–429 (2021)
4. Groß, C., Strempel, T.K.: On generalizations of conics and on a generalization of the Fermat-Torricelli problem. Am. Math. Mon. **105**(8), 732–743 (1998)
5. Halíř, R., Flusser, J.: Numerically stable direct least squares fitting of ellipses. In: 6th International Conference in Central Europe on Computer Graphics and Visualization (WSCG), pp. 125–132 (1998)
6. Hladůvka, J.: Eggfit: an iterative algorithm to fit egg-shapes to object boundaries. Software stack, TU Wien (2024). https://doi.org/10.48436/d17s6-p5d44
7. Kanatani, K., Sugaya, Y., Kanazawa, Y.: Ellipse Fitting for Computer Vision: Implementation and Applications. Springer, Heidelberg (2016). https://doi.org/10.1007/978-3-031-01815-2
8. Köhntopp, D., Lehmann, B., Kraus, D., Birk, A.: Segmentation and classification using active contours based superellipse fitting on side scan sonar images for marine demining. In: IEEE International Conference on Robotics and Automation, pp. 3380–3387 (2015)
9. Kothari, R.S., Chaudhary, A.K., Bailey, R.J., Pelz, J.B., Diaz, G.J.: Ellseg: an ellipse segmentation framework for robust gaze tracking. IEEE Trans. Visual Comput. Graphics **27**(5), 2757–2767 (2021)
10. Liao, M., et al.: Automatic segmentation for cell images based on bottleneck detection and ellipse fitting. Neurocomputing **173**, 615–622 (2016)
11. Loncaric, S.: A survey of shape analysis techniques. Pattern Recogn. **31**(8), 983–1001 (1998)
12. Long, C., Hu, Q., Zhao, M., Li, D., Ouyang, Z., Yan, D.M.: A triple-stage robust ellipse fitting algorithm based on outlier removal. IEEE Trans. Instr. Meas. **72**, 1–14 (2023)
13. Nho, T.: Egg-segmentation dataset (2023). https://universe.roboflow.com/the-nho/egg-segmentation. Accessed 26 July 2023
14. Panagiotakis, C., Argyros, A.: Region-based fitting of overlapping ellipses and its application to cells segmentation. Image Vis. Comput. **93**, 103810 (2020)
15. Pelletier, V., Hladůvka, J.: Eggshapes: a collection of egg-shaped objects and their boundaries. Dataset, TU Wien (2023). https://doi.org/10.48436/de66n-2pj41
16. Taha, A.A., Hanbury, A.: Metrics for evaluating 3D medical image segmentation: analysis, selection, and tool. BMC Med. Imaging **15**, 29 (2015)
17. Wang, W., Wang, G., Hu, C., Ho, K.C.: Robust ellipse fitting based on maximum correntropy criterion with variable center. IEEE Trans. Image Process. **32**, 2520–2535 (2023)
18. Zhang, X., Rosin, P.L.: Superellipse fitting to partial data. Pattern Recogn. **36**(3), 743–752 (2003)